TMS Annual Meeting: Phase Transformation and Microstructural Evolution Symposium
Session: Scale and Subsurface Phase Transformations during High-Temperature Oxidation

Comparison of the High-Temperature Oxidation Behavior of Subsolvus and Supersolvus Treated Advanced Powder Metallurgy Disk Alloys

Chantal K. Sudbrack, Tim P. Gabb, and David R. Hull
NASA Glenn Research Center

Jonathan D Yu
Stanford University

Timothy T Gorman
University of Dayton

Acknowledgements: James Smialek, Jack Telesman, Sue Draper, Mike Nathal for valuable discussions (NASA-GRC); Analytical Science Group for experimental support (NASA-GRC); GE Engines and Honeywell International for providing samples

Funding: NASA's Aviation Safety and Fundamental Aeronautics Programs

March 6, 2012

Background

- The drive in aerospace propulsion applications towards higher turbine inlet temperatures, which should improve engine efficiency, is leading to higher disk rim temperatures.

  Currently at 650 °C → Long-range goal of 800 °C

- Advanced powder metallurgy (P/M) nickel based superalloys have been developed by industry, AFRL and NASA to address the properties needed at these elevated temperatures e.g. Alloy 10, LSHR, ME3 (R104), RR1000

- It is well-established that oxidation can reduce fatigue life in disk alloys above 650°C by accelerated crack initiation and growth at defects, however it is not well-studied yet in disk alloys at 650 °C - 800°C Protective coatings?

Turbine stage schematic

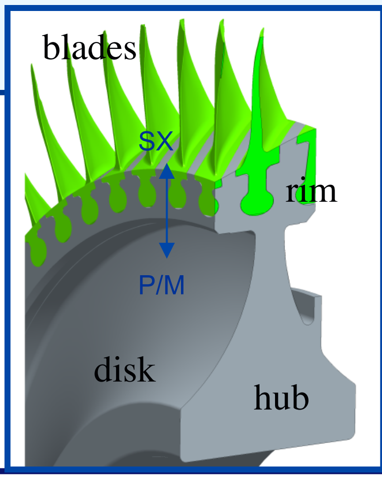

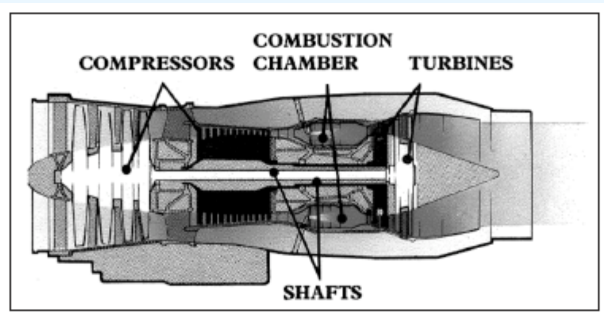

Figure 1. A schematic illustrating a cross section of a gas turbine engine.

JOM, 51:1 (1999) 14-17.

Oxidation of Disk Alloys

- Newer P/M disk alloys have substituted environmental resistance (Al, Cr levels) for strength (Mo, W, Ta, etc.)

High Cr
Low Al

Cr_2O_3 formers

Disk Alloys wt.%	Cr	Al	Cr+Al	Cr/Al	Ti
Inconel 718	19.0	0.5	19.5	38	0.9
Waspaloy	19.5	1.3	20.8	15.6	3.0
Udimet 720	18.0	2.5	20.5	7.2	2.5
RR1000	14.6	3.0	17.6	5.0	3.6
ME3	**13.0**	**3.4**	**16.4**	**3.9**	**3.8**
Alloy 10	11.5	3.5	15.0	3.3	3.5

Environmental Resistance ↑

⇐ Mechanical Properties
⇐ Temperature Capability ↓

- Stable, slow growth of **protective Cr_2O_3 external** scale with Al_2O_3 subscale by internal oxidation with fast growth **deleterious TiO_2 scale**
  - Cast-wrought disk alloy comparison shows Ti content is rate controlling

- Mass change data suggests classic parabolic growth ($time^{1/2}$) consistent with high temperature oxidation of Ni alloys for the external oxide scale

- Simplified models also predict the penetration depth of the internal oxide by precipitation to be proportional to ($time^{1/2}$)

Motivation: Environmental attack has the potential to limit turbine disk durability, particularly in next generation engines which will run hotter.

Understand environmental attack and its effect on the fatigue resistance of disk alloys

Approach:

- NASA research contracts with GE and Honeywell to identify coatings with good corrosion resistance. **In-house work now underway**
- Walk before run: oxidation is ubiquitous
- Supersolvus ME3 from GE
- Subsolvus Alloy10 from Honeywell
- **Flat coupon exposures in air: 704 °C, 760 °C and 815 °C up to 2,020 hours**
- NASA progress on fatigue response published in Superalloys 2012

Notched LCF testing at 704 °C

σ_{max}=855 MPa, R(σ)= 0.05, 0.333 Hz

Each test is represented by a diamond

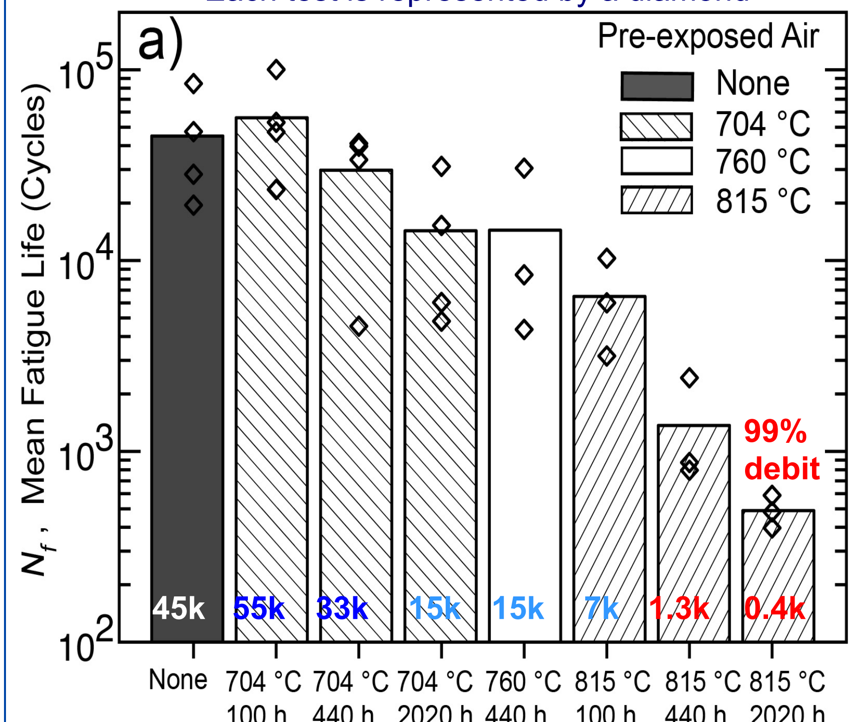

Sudbrack et al. in Superalloys 2012, 863

Dwell Notched LCF: Telesman et al. in Superalloys 2012, 853.

Both fine grained and coarse grained disks are in flight

A fine grain size provides superior yield, tensile and low cycle fatigue strength → Subsolvus heat treated

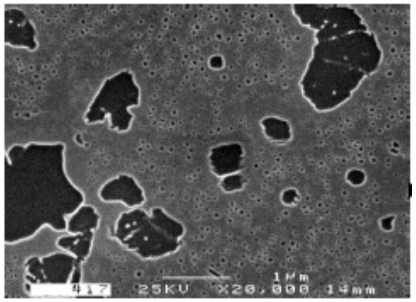

A coarse grain size provides superior creep and crack growth resistance → Supersolvus heat treated

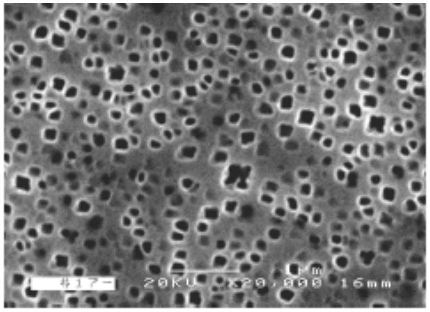

Dual-structure processing techniques to produce a fine grain bore in combination with a coarse grain web and rim offer significant benefits for advanced engine designs

Dual microstructure heat treatment (DMHT) technology

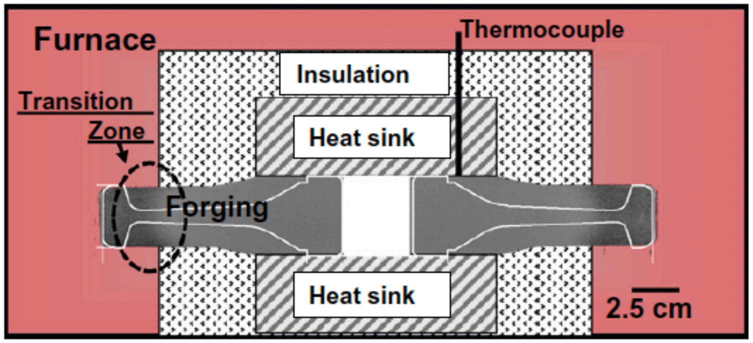

Fig. 1. Schematic of dual microstructure heat treatment (DMHT) assembly used for solution heat treatment of disk, with location of grain size transition zone indicated.

J. Gayda et al. in Superalloys 2004, 323

As-processed microstructure prior to exposures

wt.%	Cr	Co	Al	Ti	Nb	Ta	Mo	W	C	B	trace	Ni
ME3	13	21	3.4	3.7	0.8	2.4	3.8	2.1	0.05	0.02	Si, Fe, N, O, S, Zr	49.6
Alloy 10	12	19	3.4	3.5	1.4	1.4	2.5	4.6	0.03	0.03	0.06 Zr	bal

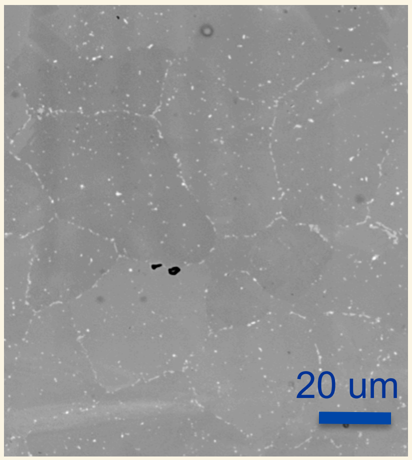

Supersolvus ME3

Grain size: 25 um – 34 um

Cr-rich $M_{23}C_6$
- carbides ornament GBs

Ti,Ta,Nb-rich MC
- carbides in interior & GBs

Volume Fraction: 0.55

Primary γ': None

Secondary γ': 190 –330 nm

Tertiary γ', 18 – 39 nm

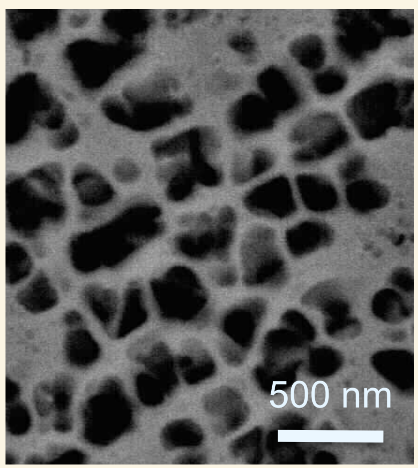

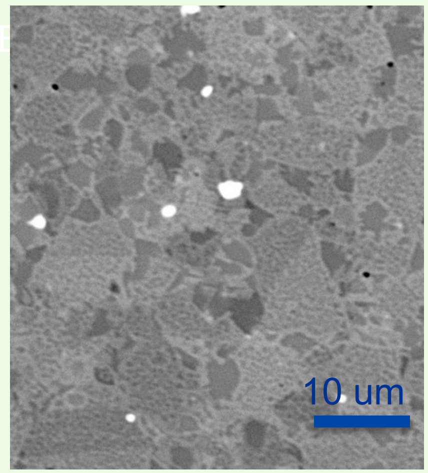

Subsolvus A10

GS: 5.26 ± 0.28 um (95%CI)

Micron sized W_3B_2

Cr-rich $M_{23}C_6$
- carbides ornament GBs

Ti,Ta,Nb-rich MC
- carbides in interior & GBs

Volume Fraction: 0.57

Primary γ': ~ 2 –5 um

Secondary γ': ~100-500 nm

Tertiary γ', ~20 –40 nm

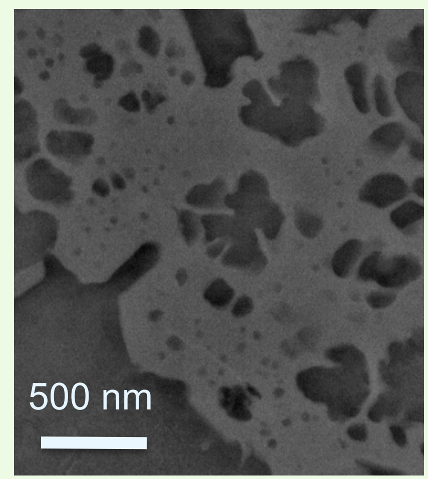

γ' ($L1_2$): Al, Ti partitioning, γ (fcc): Cr, Co, Mo partitioning

How these disk alloys oxidize

Supersolvus ME3

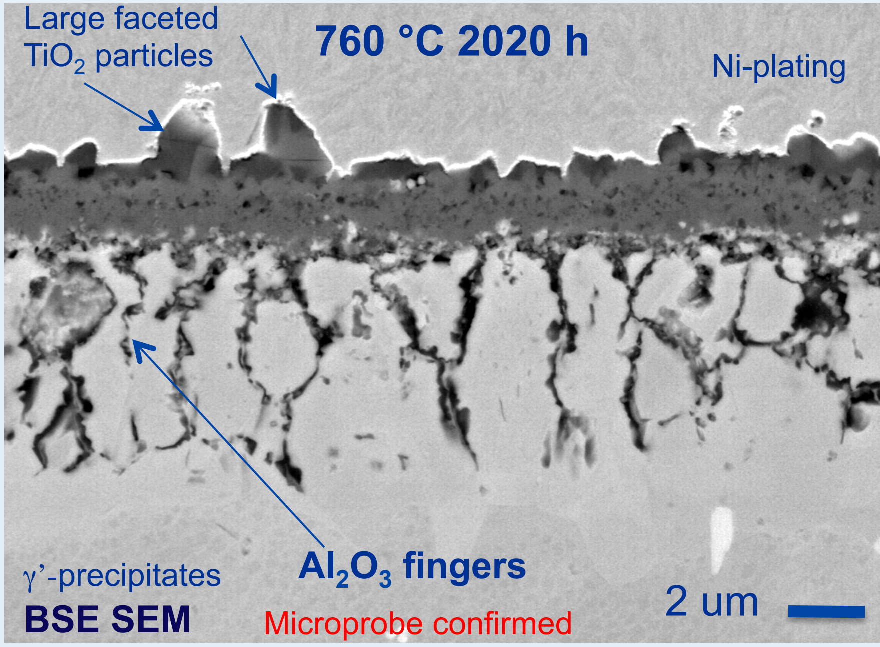

X-Ray Diffraction confirmed

Cr_2O_3+TiO_2

γ'-precipitate dissolution layer

- Cr_2O_3 external scale is intermixed with TiO_2 grains
- Ti is driven towards the surface to form primarily superficial TiO_2 grains
- Branched Al_2O_3 forms an internal oxide underneath the external scale causing γ'-precipitates to dissolve in the near surface region

Cr_2O_3 TiO_2

Plan view

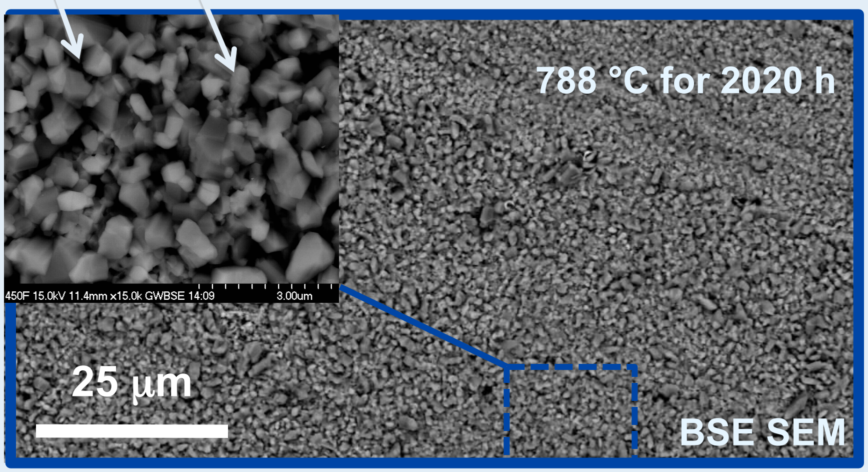

From cross sections, track evolution of

1. Cr_2O_3-TiO_2 external scale thickness
2. Al_2O_3 finger penetration depth
3. γ'-precipitate dissolution layer thickness

Simple Power Law Fit

$$y = (k \cdot t)^n$$

k **is the rate constant**

n **is the temporal exponent**

Track layer thicknesses precisely

Supersolvus ME3

704 °C for 2020 h

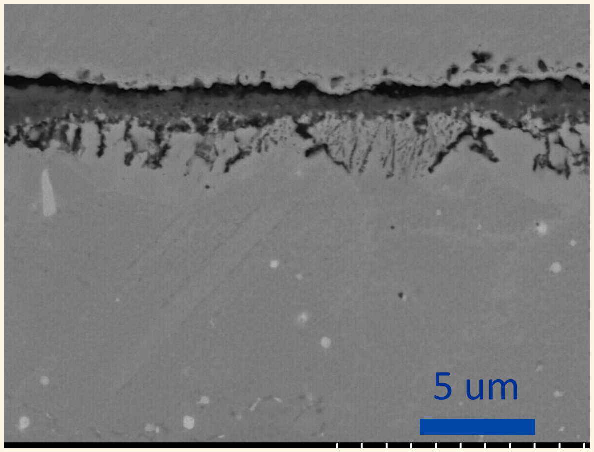

760 °C for 2020 h

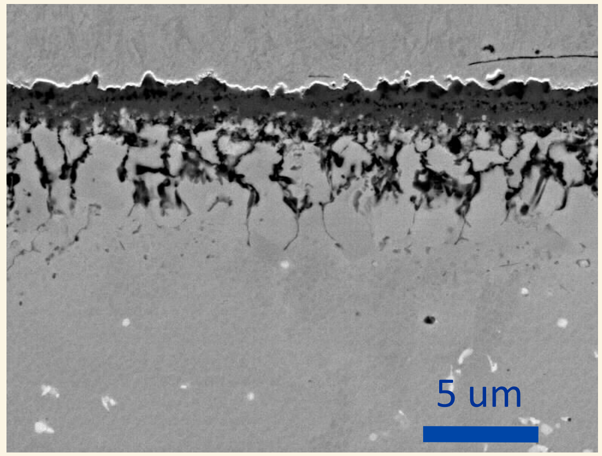

815 °C for 2020 h

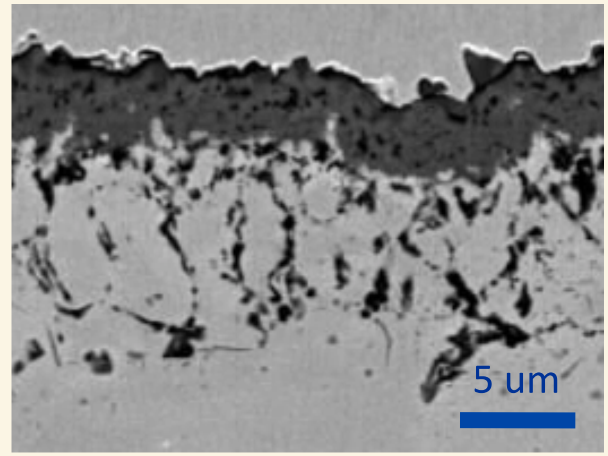

Three Areas → SEM, DIC

1. Avg. Oxide Scale Thickness (μm)
2. Avg. Al_2O_3 Finger Depth (μm)

Binary selection

ID Scale (measure thickness @ every value across)

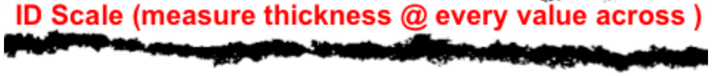

ID Al_2O_3 fingers

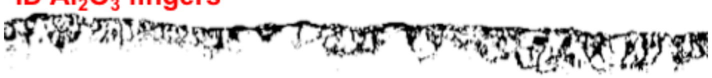

Measure extension

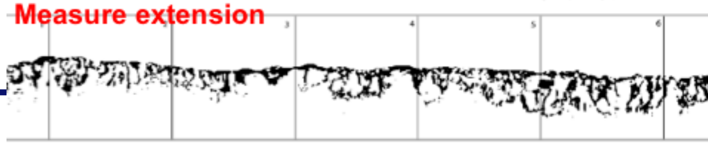

3. Avg. γ'-dissolution layer thickness (μm)

Differential Interference Contrast: 815 °C for 440 h

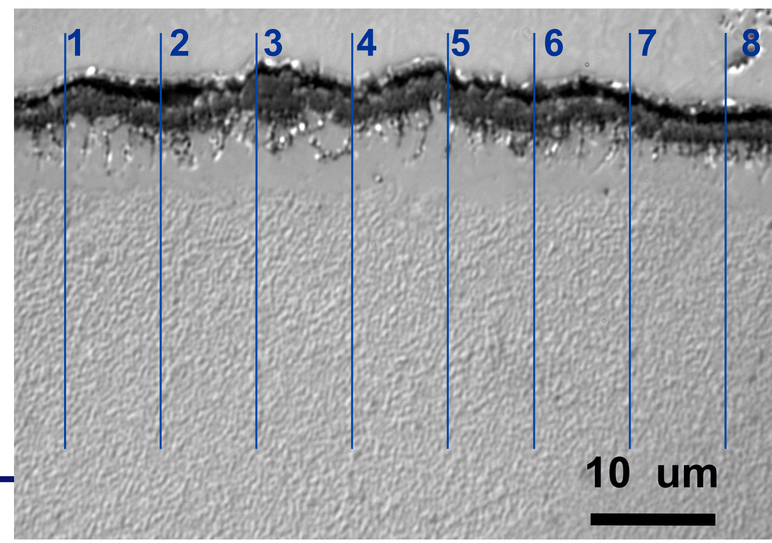

Dissolution layer

Track layer thicknesses precisely

Supersolvus ME3

704 °C for 2020 h

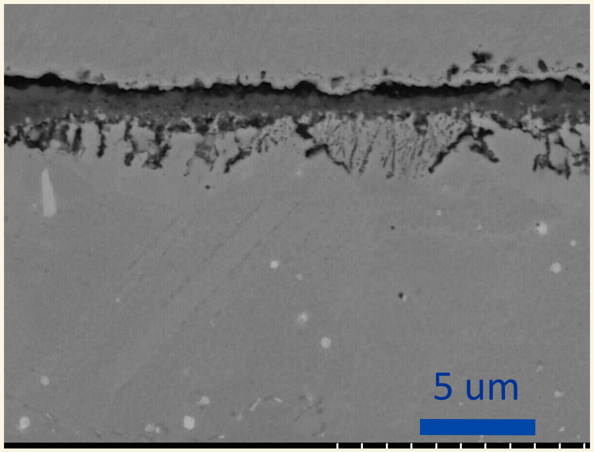

760 °C for 2020 h

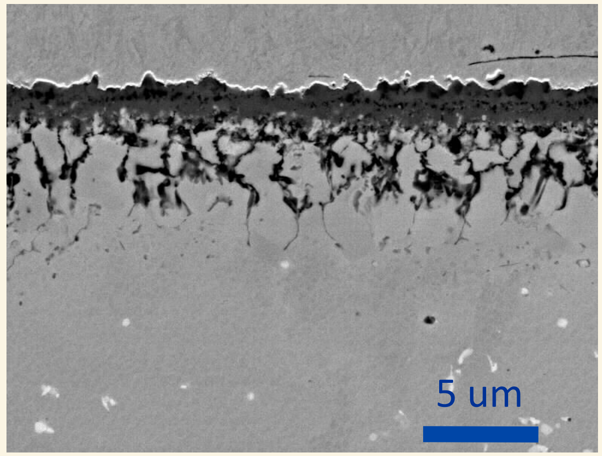

815 °C for 2020 h

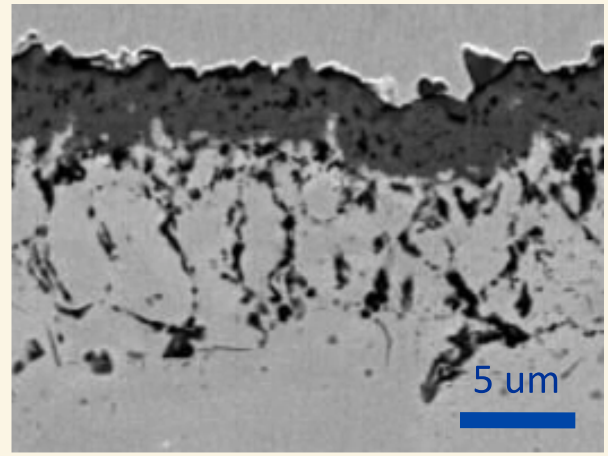

Subsolvus A10

704 °C for 2020 h

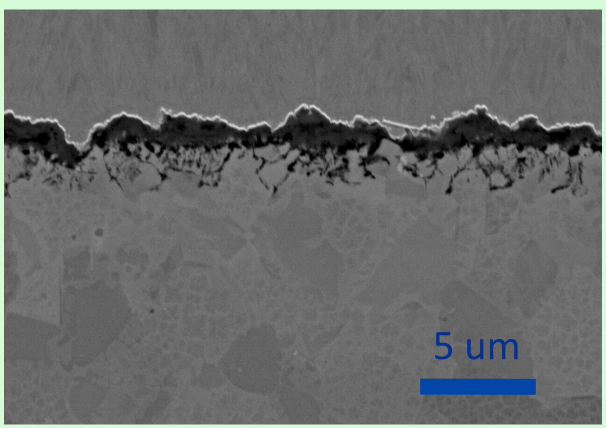

760 °C for 2020 h

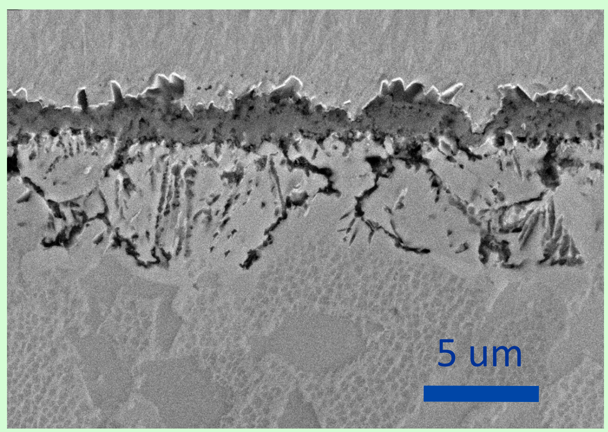

815 °C for 2020 h

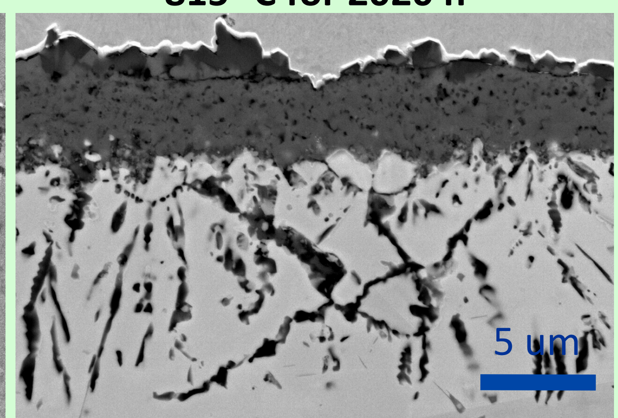

2020 h end points for three isotherms

Supersolvus ME3	Scale Thickness (um)	Alumina Penetration Depth (um)	γ'-Dissolution Layer (um)
Technique	SEM (3840)	SEM (24)	DIC (24)
Distributed	Log normal	Normal	Normal
704°C	1.32 ± 0.61	2.88 ± 0.81	3.14 ± 1.01
760°C	1.97 ± 0.67	5.23 ± 0.67	5.96 ± 1.20
815°C	3.79 ± 1.57	10.00 ± 1.16	10.75 ± 1.13

	Subsolvus A10	Scale Thickness (um)	Alumina Penetration Depth (um)	γ'-Dissolution Layer (um)
	Technique	SEM (3840)	SEM (24)	DIC (24)
	Distributed	Log normal	Normal	Normal
slower	704°C	0.69 ± 0.22	1.32 ± 0.38	–
	760°C	1.77 ± 0.14	3.97 ± 0.66	5.80 ± 1.26
compar-able	815°C	4.17 ± 0.32	9.43 ± 0.82	12.76 ± 0.60

How do the reaction kinetics compare?

Supersolvus ME3

Average Scale Thickness (um)

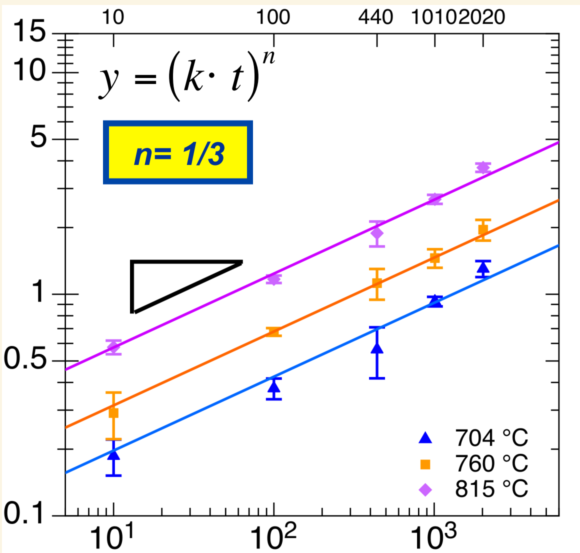

Time (h)

Average Al_2O_3 Penetration (um)

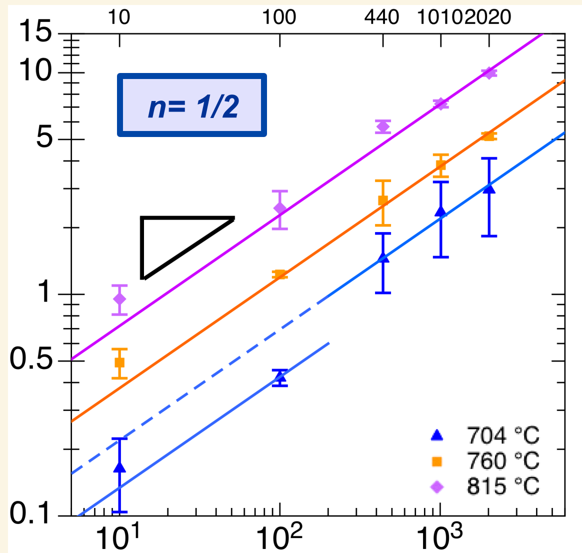

Time (h)

Average γ'-dissolution layer (um)

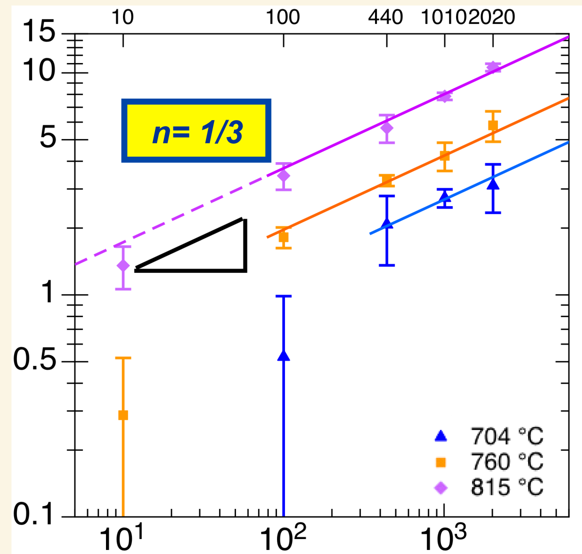

Time (h)

Scale Thickness ≤ Al_2O_3 penetration < γ'-dissolution layer

Scale Thickness	Al_2O_3 penetration	γ'-dissolution layer
k(704)=0.0077 ± 0.0018 um³/h	**k(704)upper=0.005 ± 0.004 um²/h**	**k(704)=0.019 ± 0.0010 um³/h**
k(760)=0.0031 ± 0.0006 um³/h	**k(760)=0.0142 ± 0.0011 um²/h**	**k(760)=0.076 ± 0.020 um³/h**
k(815)=0.0190 ± 0.0026 um³/h	**k(815)=0.052 ± 0.004 um²/h**	**k(815)=0.510 ± 0.008 um³/h**

- Branched Al_2O_3 penetration depth follows parabolic growth law
- Both external scale thickness and γ'-dissolution layer follow a cubic growth law
  - γ'-dissolution layer is three times thicker than external oxide scale

Grain growth in external oxide may be responsible for $t^{1/3}$ kinetics

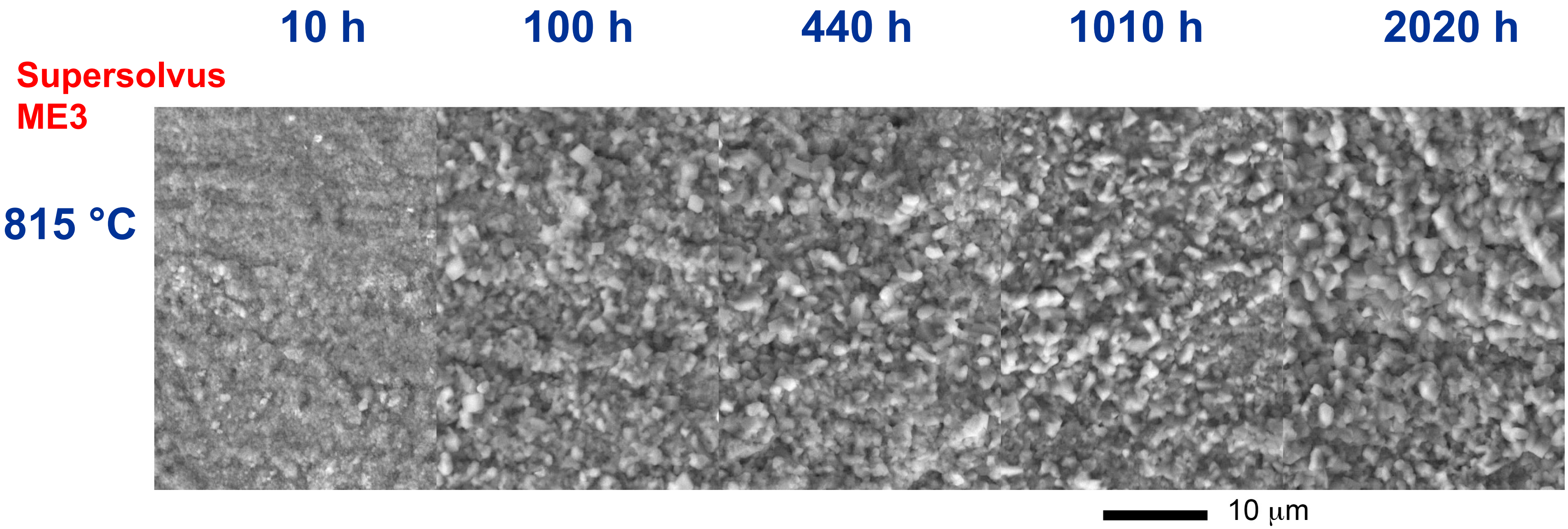

Subsolvus A10

Average Scale Thickness (um)

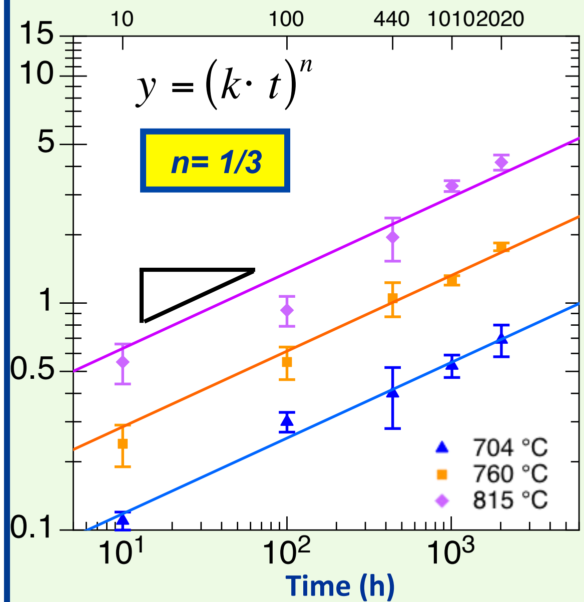

Average Al_2O_3 Penetration (um)

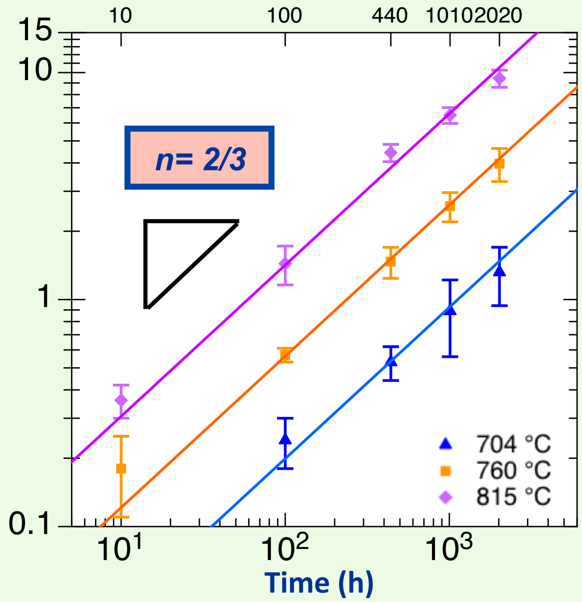

Average γ'-dissolution layer (um)

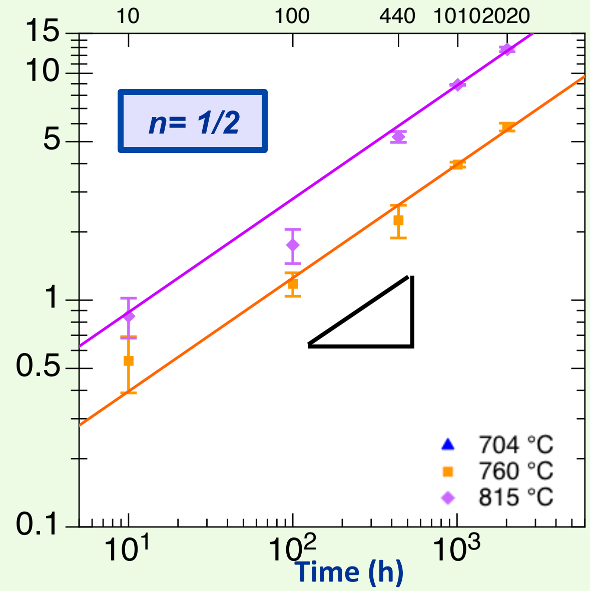

Scale Thickness > < Al_2O_3 penetration < γ'-Dissolution Layer

Scale Thickness	Al_2O_3 penetration	γ'-Dissolution Layer
k(704)=0.000164 ± 0.000026 um^3/h	k(704)= 0.00089 ± 0.00016 $um^{1.5}/h$	k(704)= Not Detected
k(760)=0.00231 ± 0.00020 um^3/h	k(760)= 0.0042 ± 0.0003 $um^{1.5}/h$	k(760)= 0.0157 ± 0.0007 um^2/h
k(815)=0.027 ± 0.003 um^3/h	k(815)= 0.0169 ± 0.0016 $um^{1.5}/h$	k(815)= 0.07818 ± 0.0008 um^2/h

Agreement: External scale thickness shows a cubic growth law

Difference: Al_2O_3 penetration depth shows larger temporal exponent→ Primary γ'-ppts.

Difference: γ'-dissolution layer evolves parabolically → short circuit diffusion

Microprobe chemical mapping: insight into diffusional processes

Supersolvus ME3: 2020 h at 815°C γ'-dissolution layer= GPD

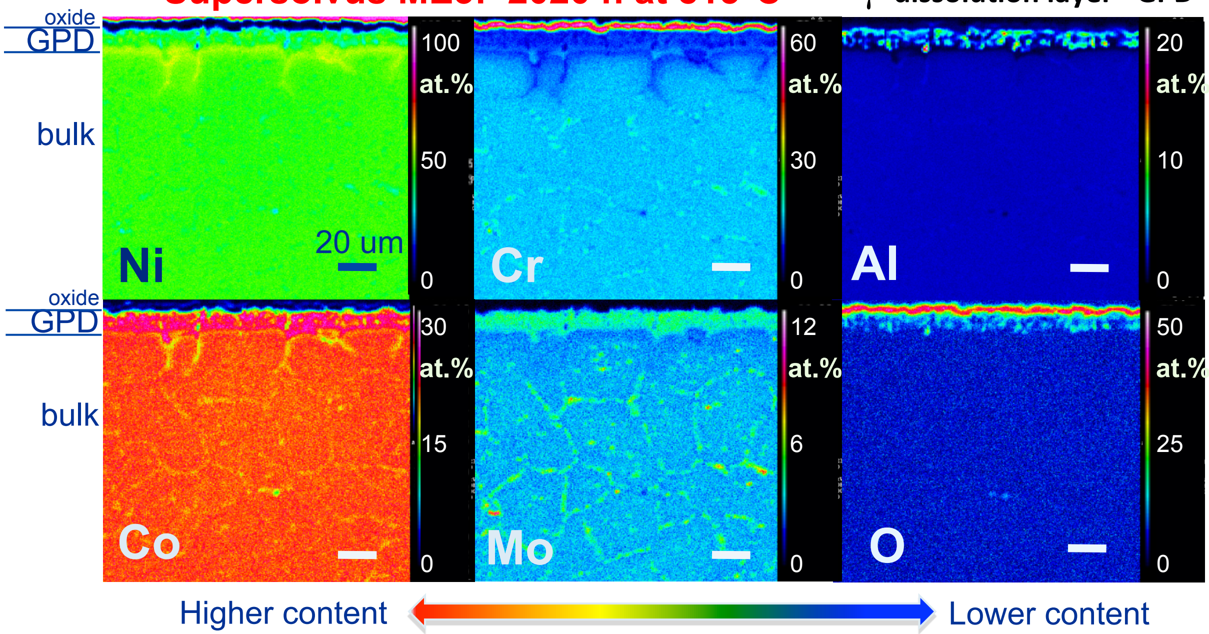

Subsolvus A10: 2020 h at 815°C γ'-dissolution layer= GPD

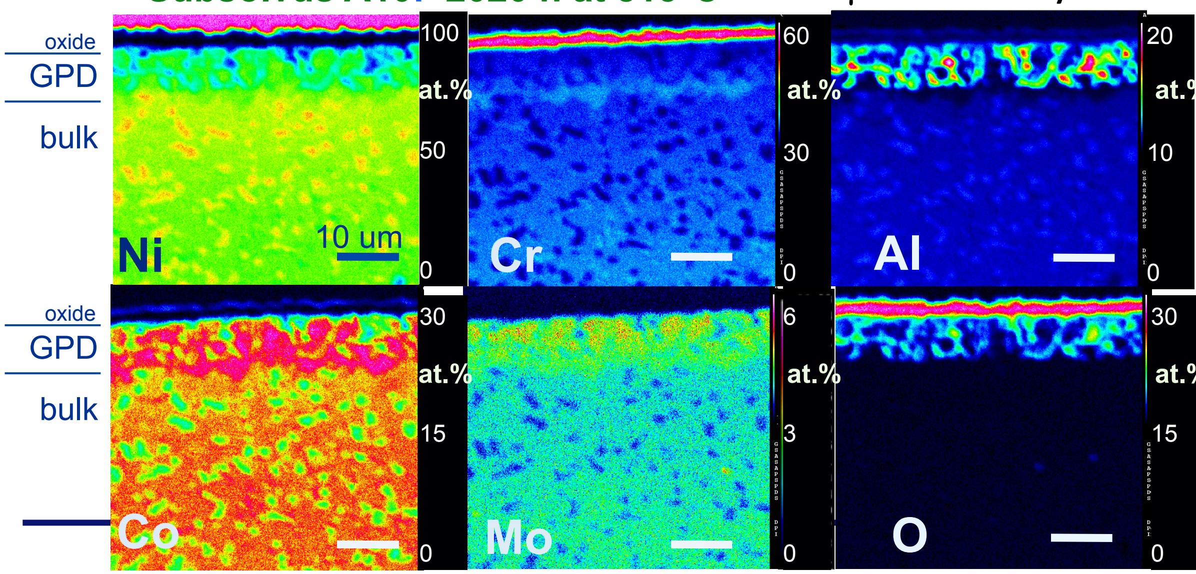

wt.%	Cr	Co	Al	Mo	C
ME3	13	21	3.4	3.8	0.05
Alloy 10	12	19	3.4	2.5	0.03

- GPD: Depletion of the major oxide elements Ti, Al, Cr, Ta
- GPD is γ-like, enriched in Co, Mo, but not Cr
- Partitioning in primary γ'
- Interfacial volume between GPD and and bulk enriched in Cr and Ti

D(Al) ≈ 3 D(Cr)

- A striking feature is the dissolution of coarsened (Cr, Mo)$_{23}$C$_6$ carbides past the GPD
  - Associated GBs are depleted in Cr, Mo and Co
- More analysis planned!

Precise layer measurements give predictive capability for fatigue life models

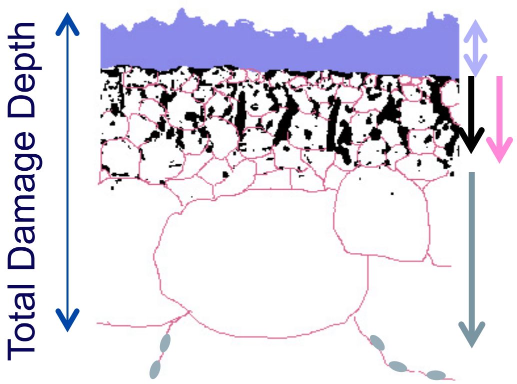

$y = \left(\kappa_1 \cdot OST\right)^{m1}$

$y = \left(\kappa_2 \cdot GPD\right)^{m2}$

$y = \left(\kappa_3 \cdot CD\right)^{m3}$

$y = \left(\kappa_4 \cdot TDD\right)^{m4}$

By substitution

$$y = \left(\kappa_n \cdot (k_n(T) \cdot t)^{1/3}\right)^{-3} \propto t^{-1}$$

Supersolvus ME3: Notched LCF data at 704 °C

Sudbrack et al. in Superalloys 2012, 863

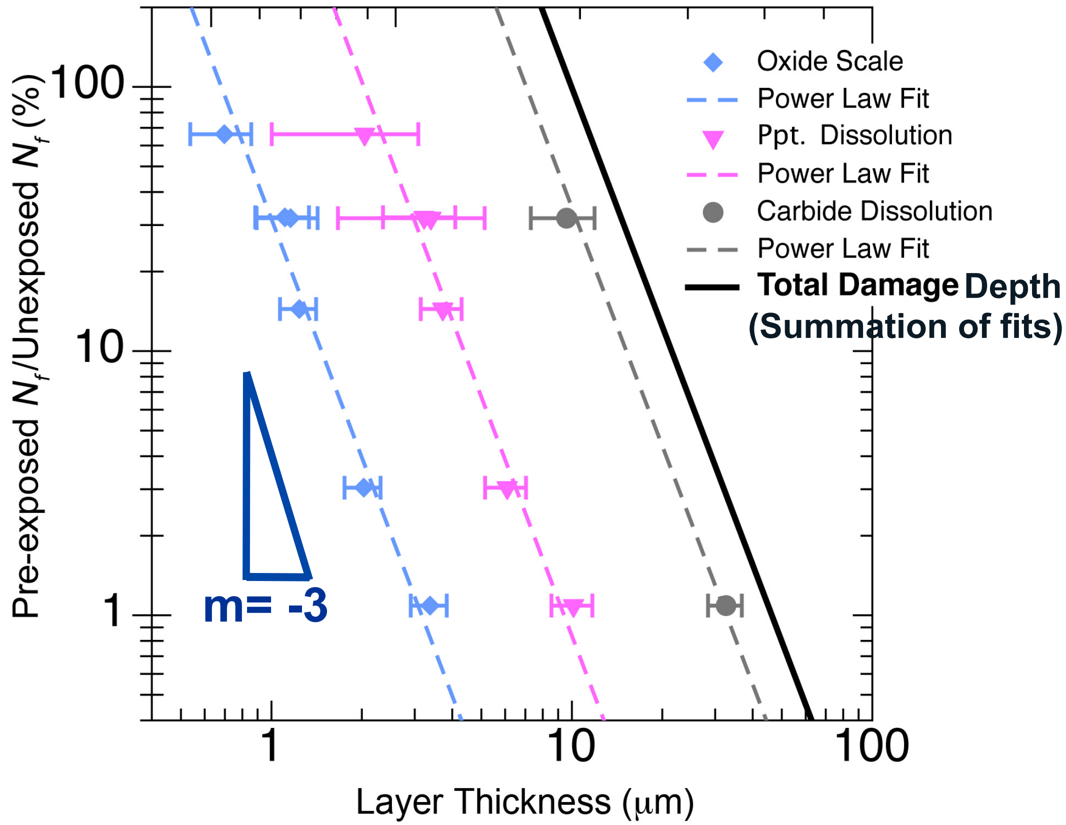

Future work → characterization of fatigue response for subsolvus Alloy 10

Conclusions

- For isothermal static oxidation of such alloys at 704 °C, 760 °C, and 815 °C**, fine-grained subsolvus disks oxidize similarly to coarse-grained supersolvus disks** despite their differences in alloy chemistry and microstructure:
  - Oxidation by-products: A continuous Cr_2O_3 external scale forms with superficial, faceted TiO_2 grains primarily at the exposed surface with an internal subscale of branched Al_2O_3 extends into a layer where the γ' -precipitates are dissolved.
  - External oxide growth: Sustained partially by dissolution of Cr-rich $M_{23}C_6$ grain boundary carbides, it has a **cubic growth** likely due to non-negligible oxide grain growth.
- However, the fine-grained subsolvus disks with primary γ'-precipitates can respond differently than coarse-grained supersolvus for:
  - Internal oxide growth: Larger temporal exponent for penetration depth of $(\text{time})^{2/3}$ for subsolvus compared to $(\text{time})^{1/2}$ for supersolvus
  - γ'-dissolution layer growth: Larger temporal exponent of $(\text{time})^{1/2}$ compared to $(\text{time})^{1/3}$
- Interestingly, over certain temperature exposures, the penetration depth of the internal oxide could be smaller for the subsolvus than supersolvus, suggesting that in addition to coarse γ'-precipitates other factors influence the growth process
  - Additional experiments: subsolvus ME3 and supersolvus Alloy 10